Journal of Hazardous Materials 187 (2011) 67–74

Contents lists available at ScienceDirect

Journal of Hazardous Materials

journal homepage: www.elsevier.com/locate/jhazmat

Application of experimental design approach and artificial neural network (ANN) for the determination of potential micellar-enhanced ultrafiltration process

Bashir Rahmanian [a], Majid Pakizeh [a], Seyed Ali Akbar Mansoori [a,*], Reza Abedini [b]

[a] Department of Chemical Engineering, Faculty of Engineering, Ferdowsi University of Mashhad, P.O. Box 91775-1111, Mashhad, Iran
[b] Department of Chemical Engineering, Faculty of Chemical Engineering, Tarbiat Modares University, P.O. Box 14115-143, Tehran, Iran

ARTICLE INFO

Article history:
Received 10 October 2010
Received in revised form
29 November 2010
Accepted 30 November 2010
Available online 8 December 2010

Keywords:
Micellar-enhanced ultrafiltration (MEUF)
Artificial neural network (ANN)
Fractional factorial design
Zinc

ABSTRACT

In this study, micellar-enhanced ultrafiltration (MEUF) was applied to remove zinc ions from wastewater efficiently. Frequently, experimental design and artificial neural networks (ANNs) have been successfully used in membrane filtration process in recent years. In the present work, prediction of the permeate flux and rejection of metal ions by MEUF was tested, using design of experiment (DOE) and ANN models. In order to reach the goal of determining all the influential factors and their mutual effect on the overall performance the fractional factorial design has been used. The results show that due to the complexity in generalization of the MEUF process by any mathematical model, the neural network proves to be a very promising method in compared with fractional factorial design for the purpose of process simulation. These mathematical models are found to be reliable and predictive tools with an excellent accuracy, because their AARE was ±0.229%, ±0.017%, in comparison with experimental values for permeate flux and rejection, respectively.

1. Introduction

The discharge of organic and metal pollutants into the environment is a serious problem due to its impact on human health and natural environment [1]. These pollutants are highly toxic, non-biodegradable and probably have a carcinogenic effect. Aqueous streams containing heavy metals are frequently encountered in industrial effluents and the sources of Cu^{2+}, Pb^{2+}, Zn^{2+} and Cd^{2+} are very common in the electroplating facilities, electrolytic refining plants, semi-conductor manufacturing and acid mine waters, among others [2].

An increasing demand for fresh water along with the larger amounts of wastewater generation due to increase in the world population and development of industrial applications, makes the recycling of the wastewaters an imperative issue [3]. For many years, many technologies such as precipitation, solvent extraction, zeolite and activated carbon adsorption, crystallization, evaporation, flotation and flocculation–coagulation are used to remove of heavy metals [4], but the traditional techniques for the removal of metal ions from aqueous effluents have their own drawbacks, such as secondary pollution of deposition, inconvenient operation, high cost, difficulty of recycling metal ions and so on [5].

Membrane processes provide a viable alternative for heavy metal recovery, as they can achieve high permeate fluxes and high rejection coefficients with low energy costs and under mild operational conditions [6]. As for the membrane cut-off to be used to remove metal ions, nanofiltration or reverse osmosis membranes should be employed, but a very high transmembrane pressure is required, rendering the process very expensive [7].

Microfiltration (MF) or traditional ultrafiltration (UF) are usually limited to the separation of molecules with high molecular weights and are not sufficient to retain all the contaminants [8]. A new and alternative approach combines several of these processes that involve binding the metals firstly to a special bonding agent (hybrid processing) [9]. Micellar-enhanced ultrafiltration (MEUF) is the one of the alternatives for the conventional metal removal technologies [10]. MEUF involves the addition of a surfactant above the critical micellar concentration (CMC) in order to entrap ionic solutes in an aqueous stream [11]. The increased hydrodynamic size of the solutes enables their rejection by ultrafiltration membranes with a cut-off in the range of 10–30 kDa [12]. The advantages of this method are the high removal efficiency, low energy consumption and small space requirement due to its high packing density [13].

Abbreviations: ANN, Artificial neural network; ARE, Average relative error; AARE, Absolute average relative error; SD, Standard deviation; MEUF, Micellar-enhanced ultrafiltration; CMC, Critical micellar concentration; 2FI's, Two-factor interactions; ANOVA, Analysis of the variance; RSM, Response surface methodology; TMP, Transmembrane pressure (bar).

* Corresponding author at: Department of Chemical Engineering, Faculty of Engineering, Ferdowsi University of Mashhad, Azadi Square, Vakilabab Boulevard, Mashhad, Iran. Tel.: +98 511 8816840; fax: +98 511 8816840.
E-mail addresses: bashir_rahmanian@yahoo.com (B. Rahmanian), pakizeh@um.ac.ir (M. Pakizeh), bidad_kavir@yahoo.com (S.A.A. Mansoori), r.abedini@modares.ac.ir (R. Abedini).

0304-3894/$ – see front matter © 2010 Elsevier B.V. All rights reserved.
doi:10.1016/j.jhazmat.2010.11.135

Nomenclature

Symbol	
R	filtration efficiency
C_p	concentration of Zn^{2+} (mg/L) in the feed solution (mM)
C_f	concentration of Zn^{2+} in the permeate (mg/L)
P_i	inlet pressure (bar)
P_o	outlet pressure (bar)
P_p	permeate pressure (bar)
Q	permeate volume (m^3)
A	area of membrane (m^2)
Jp	permeation flux (lit/m^2 min)

Most of the previous researches on MEUF usually involve the use of one-factor-at-a-time experimental approach which is not only time consuming and also excessive in cost. Also, use of conventional methods of experimentation neglect the effect of interaction between factors and leading to low efficiency in process optimization. The application of statistical experimental design and neural network for membrane preparation seems to be the best methodology for MEUF process control and optimization [14]. Factorial design and response surface methodology (RSM) analysis are important tools to determine the optimal process conditions [15]. In many experimental settings, it is not desirable or feasible to assess all factors and their joint effects; thus, it is only the dominant factors that need to be or can be identified.

2. Theory

2.1. Experimental design

In this study, a two-level fractional factorial design was employed. The 2^k factorial design is particularly useful in the early stages of experimental work when many factors are likely to be investigated. As the number of factors increase in 2^k factorial design, the numbers of required runs rapidly outgrow. If the experimenter can reasonably assume that certain high-order interactions are negligible, only a fraction of the complete factorial experiment is adequate. A major use of fractional factorial design is in screening experiments. Fractional factorial designs can often identify which factors are significant by running only a fraction (subset) of a full factorial experiment. However, there will be aliasing of effects in a fractional factorial design, which may lead to some ambiguities in interpreting the results of a designed experiment. One method for de-aliasing low-order effects is to run a follow-up experiment using the foldover approach. The foldover approach reverses the signs of one or more of the factors (columns) of the initial design to produce a follow-up design of equal size [16,17].

2.2. Artificial neural networks (ANNs)

A linear model is not suitable to constitute a satisfying relationship among the input variables for an MEUF process. The ANN approach seems to be completely suitable to the problems where the relations between variables are not linear and complex [18,19]. An ANN is a massively parallel distributed processor that has a natural propensity for storing experimental knowledge and making it available [20]. In this work, a multilayer neural network has been used, since it is effective in finding complex non-linear relationships. It has been reported that multilayer ANN models with only single hidden layer are universal approximations [21]. Hence, a three-layer feed forward neural network and the logsig processing function have been used. Preliminary numerical experiments did not show any advantage of double hidden layer network over a single hidden layer network. The results suggested that five neurons in the hidden layer were optimum and therefore it was selected to train the networks. The network was trained using Lavenberg–Marquardt (LM) algorithm. Typical network architecture is shown in Fig. 1.

The inputs to a neuron include its bias and the sum of its weighted input. The output of a neuron depends on the neuron's inputs and on its transfer function. The indices j, k, and l refer to the input signals ($j = 1, \ldots, m$) in the input layer, the neurons ($k = 1, \ldots, p$) in the hidden layer, and the neuron ($l = 1, \ldots, q$) in the output layer, respectively. There were five neurons ($m = 5$) in the input layer, five neurons ($p = 5$) in the hidden layer, and one neuron ($q = 1$) in the output layer. The transfer function, $\varphi(\upsilon_k)$ in the hidden layer was a hyperbolic tangent (Eq. (4)) and a linear function was used in the output layer (Eq. (6)). The nonlinear hyperbolic tangent function can be calculated as follows:

$$y_k = \varphi(\upsilon_k) = \frac{1 - \exp(\upsilon_k)}{1 + \exp(\upsilon_k)} \quad (1)$$

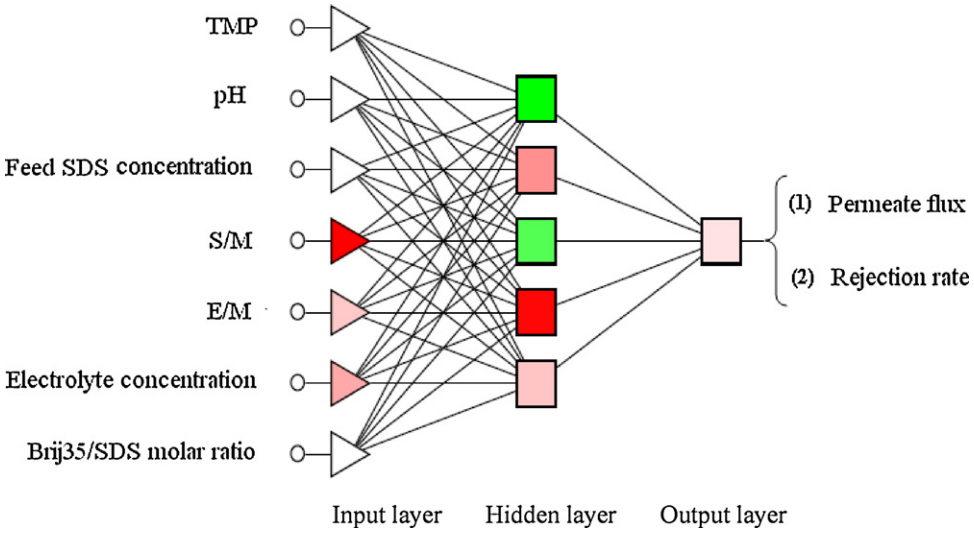

Fig. 1. A typical neural network architecture for seven input variables.

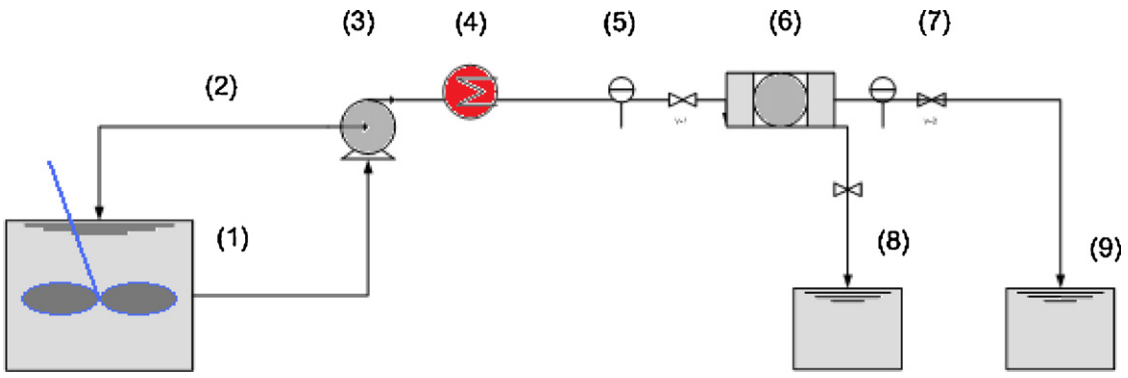

Fig. 2. MEUF experimental setup: (1) feed reservoir with stirrer, (2) bypass line, (3) centrifugal pump, (4) heat exchanger (5) monometer, (6) spiral-wound ultrafiltration module, (7) pressure control valve, (8) permeate stream and (9) retentate stream.

with υ_k being computed as

$$\upsilon_k = b_k + \sum_{j=1}^{m} w_{kj} x_j \tag{2}$$

where y_k is the output of the hidden layer, $\varphi(\upsilon_k)$ is the transfer function associated with the neuron k in the hidden layer, υ_k is the sum of weighted input of neuron k, b_k is the bias, and x_j is the input signal. Use of bias b_k has the effect of applying an affine transformation in the model. A linear function can be calculated as follows:

$$y_l = \varphi(\upsilon_l) = b_l + \sum_{k=1}^{p} w_{lk} y_k \tag{3}$$

where y_l is the output of the output layer, $\varphi(\upsilon_l)$ is the transfer function associated with neuron l in the output layer, y_k is the input to the neuron l, υ_l is the sum of weighted input of neuron l, b_l is the bias, and w_{lk} is the weight connection of neuron k and neuron l.

In the present study, Micellar-enhanced ultrafiltration (MEUF) was used to remove Zn^{2+} from synthetic wastewater by using the regenerated cellulose spiral-wound ultrafiltration membrane. In order to achieve to the purpose of determination of all of the influential factors, two-factor interactions (2FI's) and prediction response variable, the fractional factorial design and ANN has been used.

Table 1
Factors and levels for foldover fractional factorial design.

Factors	Levels		
	−1	0	1
(A) Transmembrane pressure (bar)	1	2	3
(B) Solution pH	2	7	12
(C) Feed SDS concentration (mM)	2	4	6
(D) Surfactant to metal molar ratio (S/M)	5	7.5	10
(E) Ligand–zinc ratios (L/M)	0	0.5	1
(F) Electrolyte concentration (C_{NaCl}) (mM)	0	25	50
(G) Brij35/SDS molar ratio	0	0.25	0.5

3. Materials and methods

All chemicals involved in the experiments were of analytical reagent grade. The two surfactants used were sodium dodecyl sulfate (SDS) (>99% pure) and nonionic surfactant Polyoxyethyleneglycol dodecyl ether (Brij-35) were purchased from Merck Company. Zinc ions were from zinc chloride ($ZnCl_2$) and other inorganic chemicals: (HCl, NaOH and NaCl) were all supplied by PANREAC, at analytical reagent grade. In this study, ethylenediaminetetraacetic acid (EDTA) as a ligand with a molecular weight of 372.24 was obtained from Merck Company. Distilled water was used in preparing all solutions. Distilled water produced by a water purification system (Labconco, Iran) was used in all experiments.

The ultrafiltration experiments were carried out in a cross-flow ultrafiltration unit. An UF spiral-wound of Amicon regenerated cel-

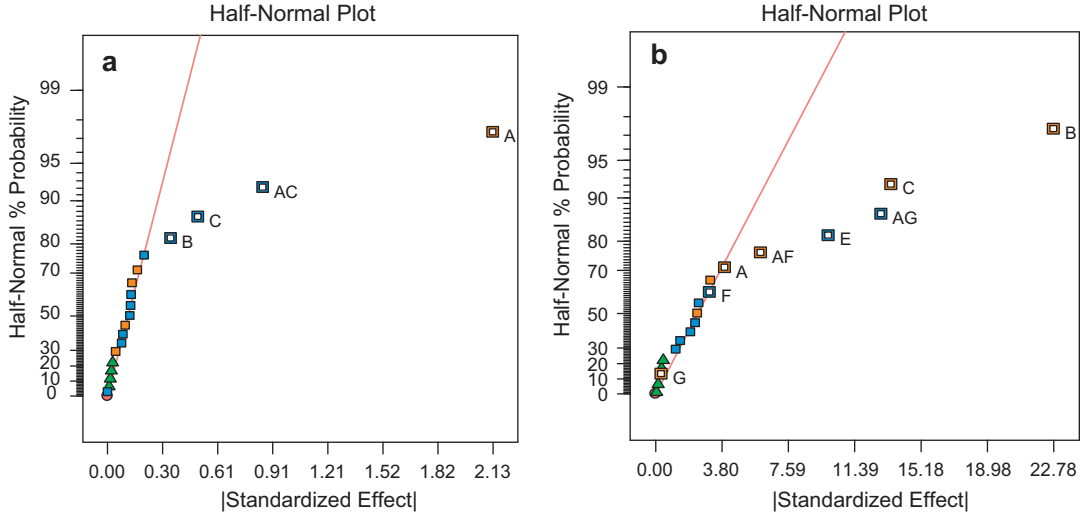

Fig. 3. A half-normal probability plot for permeate (a) and for rejection (b).

Table 2
Design layout and experimental results of 2^{7-4}_{III} fractional factorial design.

Factor input variables										Response variables	
Std.	Run	Block	*P* (bar)	pH	C_{SDS} (mM)	S/M	L/M	C_{NaCl}	$C_{Brij-35}/C_{SDS}$	Permeate flux	Rejection
1	5	1	1	2	2	10	1	50	0	1.45	44.02
2	8	1	3	2	2	5	0	50	0.5	4.52	69.86
3	10	1	1	12	2	5	1	0	0.5	0.94	92.52
4	1	1	3	12	2	10	0	0	0	4.19	96.09
5	2	1	1	2	6	10	0	0	0.5	1.44	94.2
6	11	1	3	2	6	5	1	0	0	3.05	83.49
7	9	1	1	12	6	5	0	50	0	1.92	97.94
8	7	1	3	12	6	10	1	50	0.5	2.68	90.4
9	4	1	2	7	4	7.5	0.5	25	0.25	2.46	98.75
10	6	1	2	7	4	7.5	0.5	25	0.25	2.61	96.45
11	3	1	2	7	4	7.5	0.5	25	0.25	2.52	92.14

Table 3
Design layout and experimental results of 2^{7-4}_{III} foldover fractional factorial design.

Factor input variables										Response variables	
Std.	Run	Block	*P* (bar)	pH	C_{SDS} (mM)	*S*/*M*	*L*/*M*	C_{NaCl}	$C_{Brij-35}/C_{SDS}$	Permeate flux	Rejection
12	21	2	3	12	6	5	0	0	0.5	3.18	94.2
13	20	2	1	12	6	10	1	0	0	1.83	86.67
14	13	2	3	2	6	10	0	50	0	3.66	85.29
15	12	2	1	2	6	5	1	50	0.5	2.31	66.78
16	17	2	3	12	2	5	1	50	0	4.36	90.74
17	18	2	1	12	2	10	0	50	0.5	1.57	87.59
18	16	2	3	2	2	10	1	0	0.5	4.93	50.83
19	15	2	1	2	2	5	0	0	0	2.11	59.46
20	14	2	2	7	4	7.5	0.5	25	0.25	2.89	97.84
21	22	2	2	7	4	7.5	0.5	25	0.25	2.54	93.32
22	19	2	2	7	4	7.5	0.5	25	0.25	2.4	96.65

Table 4
ANOVA for selected factorial model (response: permeate flux).

Source	Sum of squares	*df*	Mean square	*F* value	Prob > *F*	
Block	0.727272727	1	0.727272727			
Model	22.493725	4	5.62343125	105.6801185	<0.0001	Significant
Curvature	0.155461364	1	0.155461364	2.92155707	0.1080	Not significant
Residual	0.798177273	15	0.053211818			
Lack of fit	0.659377273	11	0.059943388	1.727475171	0.3158	Not significant
Pure error	0.1388	4	0.0347			
Cor. total	24.17463636	21		*R*-squared	0.96	
				Adj *R*-squared	0.95	
				Adeq precision	28.99	

lulose (PL series, Millipore) with an effective area of 0.5 m^2 was used. The membrane cut-off was 20 kDa. The aqueous mixture was stirred at a constant speed of 300 rpm. After being fully mixed, the solution was fed into the membrane module in continuous and cross-flow mode of ultrafiltration by centrifugal pump. The temperature was kept at 25 ± 2 °C in all experiment. A schematic of the MEUF is shown in Fig. 2.

After each run, the membrane was thoroughly washed by NaOH, HCl and distilled water for at least 15 min and at a pressure of 4 bar. The membrane permeability was checked to ensure that the permeability remains almost constant between successive runs. After each step in the cleaning procedure, distillated water was circulated at 3 bar and room temperature, until the pH of the permeate flux became neutral. Before each run, ultrapure water was filtered in order to determine the permeability and to check the membrane.

CMC of SDS and Brij-35 were determined 8.15 mM and 0.36 mM using the conductivity meter and surface tension method, respectively.

Table 5
ANOVA for selected factorial model (response: rejection rate).

Source	Sum of squares	*df*	Mean square	*F* value	Prob > *F*	
Block	98.24182273	1	98.24182273			
Model	4108.500575	8	513.5625719	32.86290225	<0.0001	Significant
Curvature	1011.936594	1	1011.936594	64.75388821	<0.0001	Significant
Residual	171.9016856	11	15.62742596			
Lack of fit	138.4038189	7	19.77197413	2.360983084	0.2123	Not significant
Pure error	33.49786667	4	8.374466667			
Cor. total	5390.580677	21		*R*-squared	0.78	
				Adj *R*-squared	0.63	
				Adeq precision	7.86	

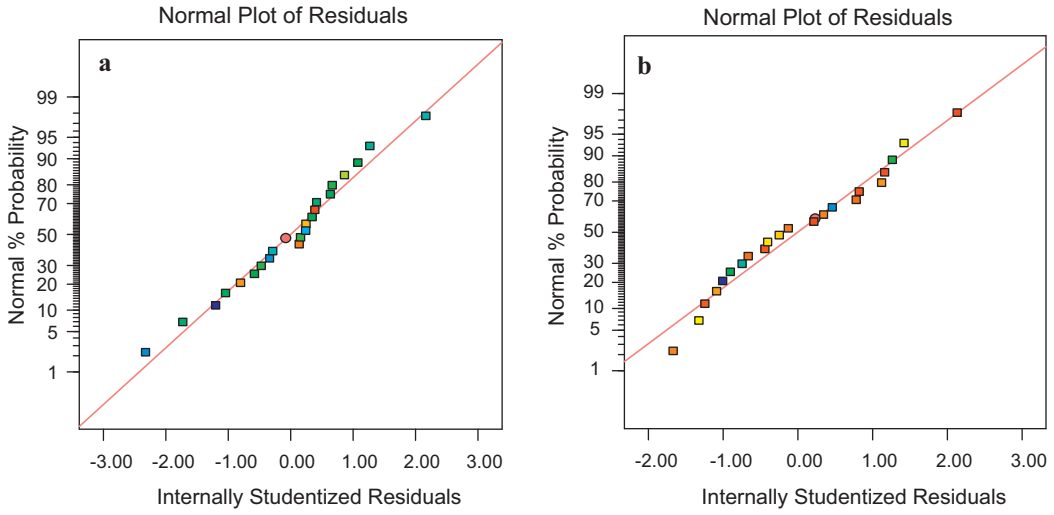

Fig. 4. Normal probability plot of residual for permeate flux (a) and rejection rate (b).

To evaluate the filtration efficiency in removal of chromate and nitrate from the feed solution, the following equation was used:

$$R = 1 - \frac{C_p}{C_f} \tag{4}$$

C_f is the concentration of Zn^{2+} (mg/L) in the feed solution; C_p (mg/L) is the concentration of Zn^{2+} in the permeate (mg/L).

TMP is the transmembrane pressure which can be calculated by the following equation:

$$\text{TMP} = \tfrac{1}{2}(P_i + P_o) - P_p \tag{5}$$

where P_i, P_o and P_p are inlet, outlet and permeate pressures, respectively.

Table 1 presents the variables of interest and their real values at the levels set in the design. Each factor at two levels (high, +1 and low, −1 levels), the center points (coded level 0), which is the midpoint between the high and low levels, is repeated thrice.

The exploration of the experimental domain is started with a fractional factorial design, consisting of 8 experiments, whose extreme values are reported in Table 2. Three replicates of the central experiment were performed along the fractional factorial design in order to check the analysis repeatability and to estimate the experimental error.

This design is a 1/16th fraction, so every effect will be aliased with 15 other effects, most of which are ignored by default to avoid unnecessary screen clutter. The output indicates that each main effect will be confounded with three two-factor interactions. The aliases structure for 2^{7-4}_{III} design indicates as below:

[A] = A + BD + CE + FG
[B] = B + AD + CF + EG
[C] = C + AE + BF + DG
[D] = D + AB + CG + EF
[E] = E + AC + BG + DF
[F] = F + BC + AG + DE
[G] = G + CD + BE + AF

We recognize out that all the main effects in this design are confounded with two-factor interactions. Maybe one of those confounded interactions is actually what is important. You must run at least one more experiment to clear this up. To untangle the main effects from the interactions in its initial resolution III design, can run a "foldover," which requires a reversal in all of the signs on the original eight runs [16]. Combining both blocks of runs produces a resolution IV design in which all of the main effects will be free and clear of two-factor interactions (2FI's). However, all the 2FI's remain confounded with each other [17]. Data set of fractional factorial with foldover experimental design used, reported in Table 3.

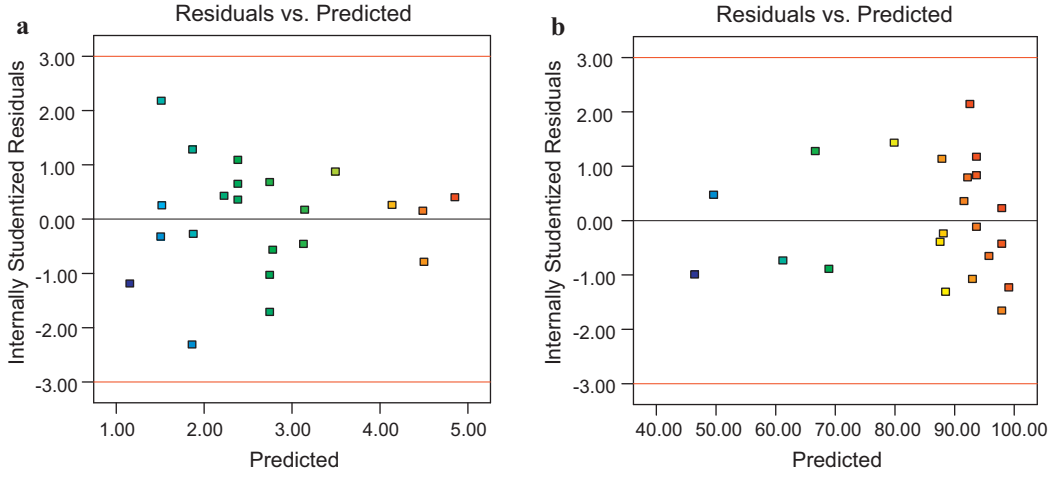

Fig. 5. Plot of residual vs. predicted response for permeate flux (a) and rejection rate (b).

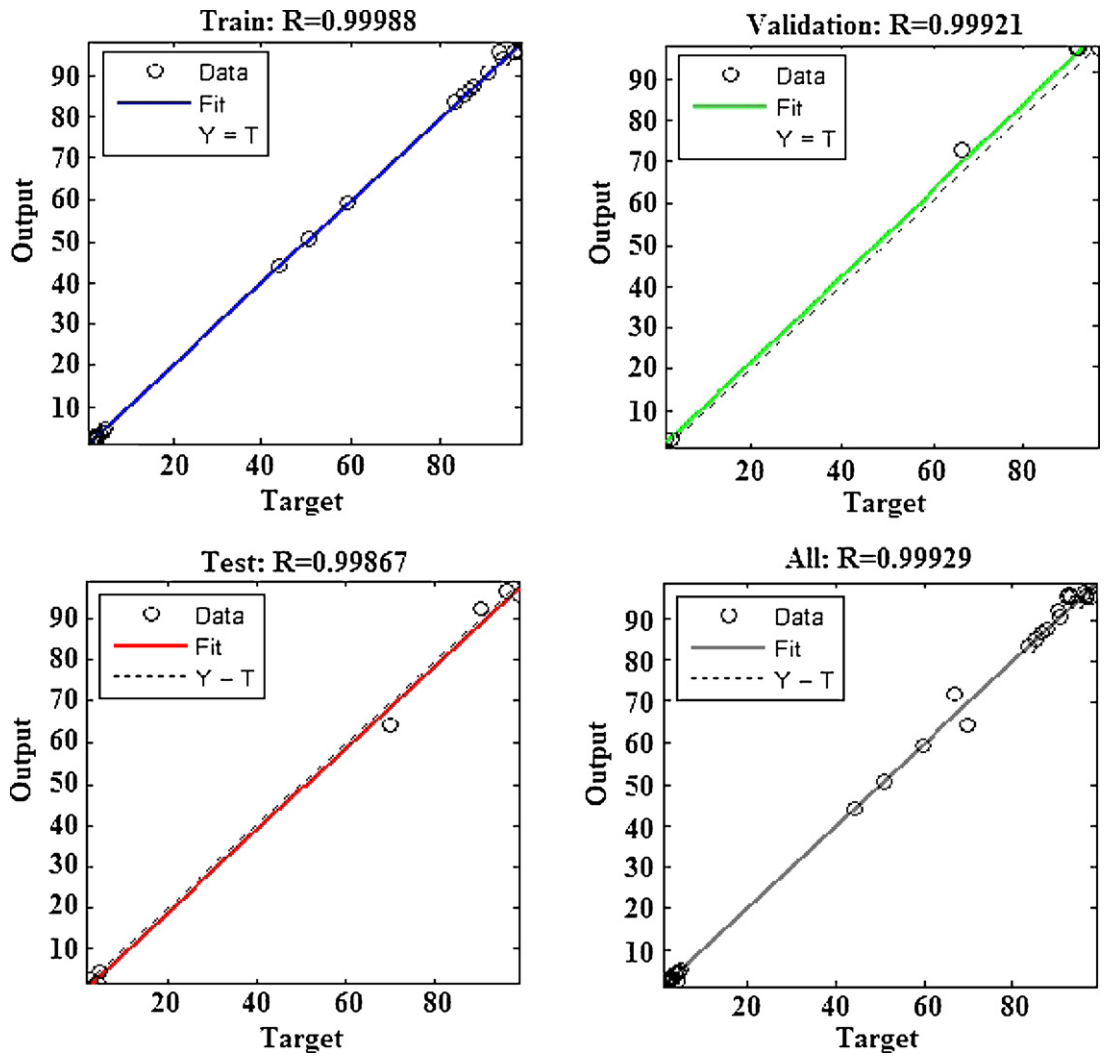

Fig. 6. Network model with training, validation, test and all prediction set.

4. Result and discussion

4.1. Half-normal probability plot

Quantitatively, the estimated effects of a given main effect or interaction and its rank relative to other main effects and interactions is given via least squares estimation (that is, forming effect estimates that minimize the sum of the squared differences between raw data and the fitted values from such estimates). Having such estimates in hand, one could then construct a list of the main effects and interactions ordered by the effect magnitude. The half-normal probability plot is a graphical tool that uses these ordered estimated effects to help assess which factors are important and which are unimportant. The half-normal probability plot of the effects for responses data set is as follows:

Fig. 3 is a normal probability plot of the effects. All the effects that lie along the line were negligible, whereas larger ones are far from the line. Hence, the main effects including the transmembrane tressure (A), solution pH (B) and feed SDS concentration (C) and AC as the interaction effect significantly influenced the permeate flux, whereas the solution pH (B), feed SDS concentration (C), the interaction effect between the transmembrane tressure and the Brij35/SDS molar ratio (AG), Ligand–zinc ratios (E) and the interaction between the transmembrane pressure and the electrolyte concentration (AF) were significant for rejection responses within the levels and conditions tested.

The main effects including the Brij35/SDS molar ratio (G) and the electrolyte concentration (F) were not a significant term, but to present a hierarchic model they were included in the model. Model hierarchy maintains the relationships between the main and interaction effects.

4.2. Data analysis

The data analysis was performed using Design-Expert Version 8.0.4 statistical software. The fitted models were assessed with the coefficient of determination, R^2. A concern with this statistic is that it always increases as terms are added to the model, even though the added terms are often not significant. Consequently, this statistic is usually smaller for the refined model in comparison with corresponding full model. To negate this drawback, the adjusted coefficient of determination, R^2-Adj; is used. This statistic is adjusted to the size of the model, more specifically, the number of factors. The addition of nonsignificant terms to the model can usually decrease the R^2 Adj: value [22].

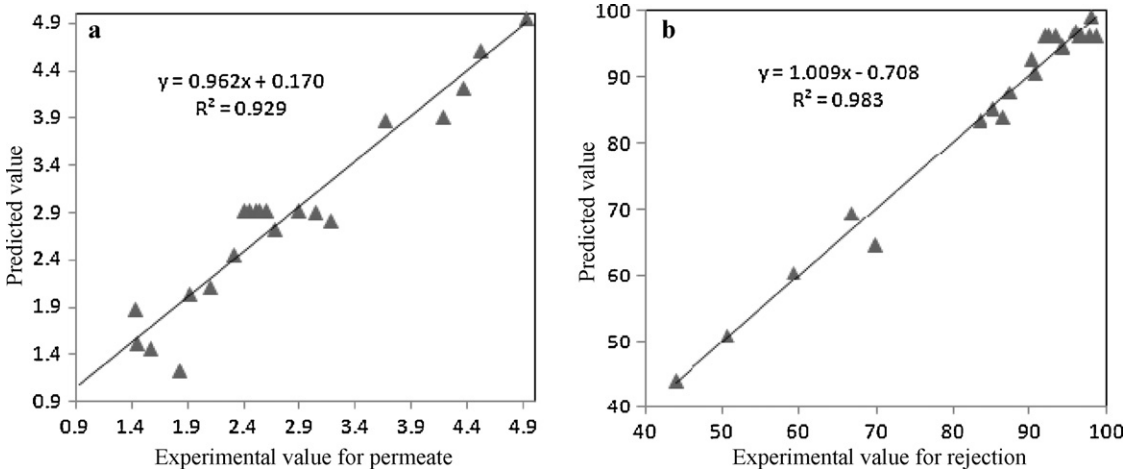

Fig. 7. Correlation between experimental and predicted values of (a) permeate flux response and (b) rejection rate responses using ANN.

4.2.1. ANOVA analysis

In order to ensure a good model, test for significance of the regression model, test for significance on individual model coefficients and test for lack-of-fit must be performed. An ANOVA table is commonly used to summarize the tests that were performed. Table 4 shows the ANOVA table for rejection rate response.

The *R*-squared calculated is 0.96, reasonably close to 1, which is acceptable. It implies that about 96% of the variability in the data is explained by the model. Adequate precision compares the range of the predicted values at the design points to the average prediction error. The ratios greater than 4 indicate adequate model discrimination. In this case, the value is well above 4. The lack-of-fit *P* value of 0.3158 showed that the lack of fit was not important relative to the pure error. The lack-of-fit can also be said to be insignificant. This is desirable as we want a model that fits.

The same procedure is applied on the other response variable, rejection rate and the resulting ANOVA table is shown in Table 5. The *R*-squared for rejection rate is 0.78, close to 1, which is desirable. The adequate precision value is well above 5.

Also the *F*-statistics (*P*-value > 0.05) for the rejection response lack-of-fit indicated that there was an adequate goodness-of-fit.

As an additional tool to check the adequacy of the final model, the normal probability plot of the studentized residuals is illustrated in Fig. 4. The points on this plot lie reasonably close to a straight line, confirming that the errors were normally distributed with mean zero and constant. The curvature *P*-value < 0.0001 indicated that there is a significant curvature (as measured by the difference between the average of the center points and the average of the factorial points) in the design space. As a result, a linear model along with the interaction terms that gave a twisted plane was not adequate to explain the response.

Also plots of the residuals in Fig. 5 revealed that they have no obvious pattern and unusual structure. They also show equal scatter above and below the *x*-axis. This implies that the model proposed is adequate and there is no reason to suspect any violation.

Table 6
ARE, AARE and SD for permeate flux and rejection which modeled by ANN.

	Method	% ARE	%AARE	%SD
Permeate flux	ANN	−0.12519	0.229844	0.498206
Rejection (*R* %)	ANN	−0.00055	0.017281	0.026327

4.3. Artificial neural networks

Fig. 6 shows the regression plots for the output with respect to training, validation, and test data. The output tracks the targets very well, and the *R*-value is over 0.999. In this case, the network response is satisfactory.

Fig. 7 represents comparison between the predicted data by ANN model and the experimental data which have not been used in training of the ANN (1/3 remaining data). As it can be seen from Fig. 7 the ANN provides results very close to experimental measurements. The predictions which match measured values should fall on the diagonal line. Almost all data fall on this line, which confirms the accuracy of the ANN model.

Table 6 reveals average relative error (ARE), absolute average relative error (AARE) and standard deviation (SD) for the Zn^{2+} rejection percentage and the permeate flux, respectively. ARE, AARE and SD are defined as below:

$$\mathrm{ARE} = \frac{1}{N}\sum_{i=1}^{N}\left(\frac{X_{\mathrm{experimental}(i)} - X_{\mathrm{caculated}(i)}}{X_{\mathrm{experimental}(i)}}\right) \quad (6)$$

$$\mathrm{AARE} = \frac{1}{N}\sum_{i=1}^{N}\left(\left|\frac{X_{\mathrm{experimental}(i)} - X_{\mathrm{caculated}(i)}}{X_{\mathrm{experimental}(i)}}\right|\right) \quad (7)$$

$$\mathrm{SD} = \sqrt{\frac{1}{N-1}\sum_{i=1}^{N}\left(\left|\frac{X_{\mathrm{experimental}(i)} - X_{\mathrm{caculated}(i)}}{X_{\mathrm{experimental}(i)}}\right| - \mathrm{AARE}\right)^2} \quad (8)$$

Table 7 summarizes a comparison between the present work and the other methods given in the published earlier articles for

Table 7
A comparison between the present work and the other methods.

Type of process	Method	Responses variables	Statistical index	Ref.
Milk ultrafiltration	ANN	Permeate flux& the solutes rejection	Average errors < 1%	[23]
Copper removal by MEUF	RSM	Rejection coefficient	R^2 = 79.03%	[24]
Cross flow milk ultrafiltration	Fuzzy	Permeate flux& the components rejection	–	[25]
Present work	ANN	Permeate flux & the rejection rate	R^2 > 92%	

evaluation membrane performance. However, in most of them, it can be said that the empirical models developed were reasonably accurate. In present work, a multilayer neural network has been used, since it is effective in finding complex non-linear relationships for zinc removal using MEUF process according to statistical analysis.

5. Conclusions

The present study shows that experimental design and artificial neural network model can be used for the modeling of zinc removal using MEUF process. ANOVA analysis indicated that there is significant curvature in the design space. As a result, a linear model along with the interaction terms that gave a twisted plane was not adequate to explain the responses. So, a multilayer neural network has been used, as it is effective to find complex non-linear relationships. These mathematical models are found to be reliable and predictive tools with an excellent accuracy with AARE ±0.229%, ±0.017%, in comparison with experimental values for permeate flux and rejection, respectively. It was observed that there is an acceptable agreement between ANN model results with experimental data.

Acknowledgment

The authors are indebted to Department of Food Technology, Khorasan Research Institute for Food Science and Technology, Mashhad, Iran for their financial assistance and support.

References

[1] B.R. Fillipi, J.F. Scamehorn, S.D. Christian, R.W. Taylor, A comparative economic analysis of copper removal from water by ligand-modified micellar-enhanced ultrafiltration and by conventional solvent extraction, J. Membr. Sci. 145 (1998) 27–44.
[2] D. Feng, C. Aldrich, H. Tan, Removal of heavy metal ions by carrier magnetic separation of adsorptive particulates, Hydrometallurgy 56 (2000) 359–368.
[3] H. Polat, D. Erdogan, Heavy metal removal from waste waters by ion flotation, J. Hazard. Mater. 148 (2007) 267–273.
[4] T.A. Kurniawan, G.Y.S. Chan, W.-H. Lo, S. Babel, Physico-chemical treatment techniques for wastewater laden with heavy metals, Chem. Eng. J. 118 (2006) 83–98.
[5] K.G. Xu, m. Zeng, J.H. Huang, J.Y. Wu, Y.Y. Fang, G. Huang, J. Li, B. Xi, H. Liu, Removal of Cd^{2+} from synthetic wastewater using micellar-enhanced ultrafiltration with hollow fiber membrane, Colloids Surf. A 294 (2007) 140–146.
[6] J. Landaburu-Aguirre, V. Garcia, E. Pongracz, R. Keiski, Applicability of membrane technologies for the removal of heavy metals, Desalination 200 (2006) 272–273.
[7] F. Ferella, M. Prisciandaro, I.D. Michelis, F. Veglio, Removal of heavy metals by surfactant-enhanced ultrafiltration from wastewaters, Desalination 207 (2007) 125–133.
[8] E. Samper, M. Rodriguez, M.A. De la Rubia, D. Prats, Removal of metal ions at low concentration by micellar-enhanced ultrafiltration (MEUF) using sodium dodecyl sulfate (SDS) and linear alkylbenzene sulfonate (LAS), Sep. Purif. Technol. 65 (2009) 337–342.
[9] C. Blocher, J. Dorda, V. Mavrov, H. Chmiel, N.K. Lazaridis, K.A. Matis, Hybrid flotation-membrane filtration process for the removalof heavy metalions from wastewater, Water Res. 37 (2003) 4018–4026.
[10] J. Jung, J.-S. Yang, S.-H. Kim, J.-W. Yang, Feasibility of micellar-enhanced ultrafiltration (MEUF) for the heavy metal removal in soil washing effluent, Desalination 222 (2008) 202–211.
[11] K. Baek, J.W. Yang, Micellar-enhanced ultrafiltration of chromate and nitrate: binding competition between chromate and nitrate, Desalination 167 (2004) 111–118.
[12] M. Bielska, J. Szymanowski, Removal of methylene blue from waste water using micellar enhanced ultrafiltration, Water Res. 40 (2006) 1027–1033.
[13] S. Lacour, J.C. Bollinger, B. Serpaud, P. Chantron, R. Arcos, Removal of heavy metals in industrial wastewaters by ion exchanger grafted textiles, Anal. Chim. Acta 428 (2001) 121–132.
[14] M. Khayet, C. Cojocaru, M.C. Garcia-Payo, Experimental design and optimization of asymmetric flat-sheet membranes prepared for direct contact membrane distillation, J. Membr. Sci. 351 (2010) 234–245.
[15] R. Gheshlaghi, J.M. Scharer, M. Moo-Young, P.L. Douglas, Application of statistical design for the optimization of amino acid separation by reverse-phase HPLC, Anal. Biochem. 383 (2008) 93–102.
[16] K.-T. Fang, D.K.J. Lin, H. Qin, A note on optimal foldover design, Stat. Prob. Lett. 62 (2003) 245–250.
[17] M. Aia, F.J. Hickernellb, D.K.J. Linc, Optimal foldover plans for regular s-level fractional factorial designs, Stat. Prob. Lett. 78 (2008) 896–903.
[18] L. Bernard, P. Bernard, G. Karine, B. Florence, J.P. Croue, Modeling of bromated formation by ozonation of surface waters in drinking water treatment, Water Res. 38 (2004) 2185–2195.
[19] M. Yang, H. Wei, Application of a neural network for the prediction of crystallization kinetics, Ind. Eng. Chem. Res. 45 (2006) 70–75.
[20] B.D. Ripley, Pattern Recognition and Neural Networks, Cambridge University Press, Cambridge, 1996.
[21] K. Hornik, M. Stinchcombe, H. White, Multilayer feedforward neural networks are universal approximators, Neural Netw. 2 (1989) 359.
[22] F. Ani Idris, M.Y. Kormin, Noordin, Application of response surface methodology in describing the performance of thin film composite membrane, Sep. Purif. Technol. 49 (2006) 271–280.
[23] S.M.A. Razavia, S.M. Mousavi, S.A. Mortazavi, Dynamic prediction of milk ultrafiltration performance: a neural network approach, Chem. Eng. Sci. 58 (2003) 4185–4195.
[24] I. Xiarchosa, A. Jaworska, G. Zakrzewska-Trznadel, Response surface methodology for the modelling of copper removal from aqueous solutions using micellar-enhanced ultrafiltration, J. Membr. Sci. 321 (2008) 222–231.
[25] J. Sargolzaei, M. Khoshnoodi, N. Saghatoleslami, M. Mousavi, Fuzzy inference system to modeling of crossflow milk ultrafiltration, Appl. Soft Comput. 8 (2008) 456–465.